Dipyridamole enhances osteogenesis of three-dimensionally printed bioactive ceramic scaffolds in calvarial defects

Jonathan M. Bekisz, BA[1], **Roberto L. Flores, MD**[2], **Lukasz Witek, MSci, PhD**[3], **Christopher D. Lopez, BA**[3,4], **Christopher M. Runyan, MD, PhD**[2,5], **Andrea Torroni, MD**[6], **Bruce N Cronstein, MD**[7], and **Paulo G. Coelho, DDS, PhD**[2,3]

[1]New York University Langone Medical Center, 550 First Avenue, New York, NY, 10016, United States of America

[2]Hansjörg Wyss Department of Plastic Surgery, New York University Langone Medical Center, 307 East 33rd Street, New York, NY, 10016, United States of America

[3]Department of Biomaterials and Biomimetics, New York University College of Dentistry, 433 First Avenue, New York, NY, 10010, United States of America

[4]Icahn School of Medicine at Mount Sinai, 1468 Madison Avenue, New York, NY, 10029, United States of America

[5]Department of Plastic Surgery, Wake Forest Baptist Health, 1 Medical Center Blvd, Winston-Salem, NC, 27103, United States of America (Present Address)

[6]Department of Oral and Maxillofacial Surgery, New York University Langone Medical Center, 530 First Avneue, New York, NY, 10016, United States of America

[7]Department of Medicine, New York University Langone Medical Center, 550 First Avenue, New York, NY, 10016, United States of America

Summary

Purpose—The objective of this study was to test the osteogenic capacity of dipyridamole-loaded, three-dimensionally printed, bioactive ceramic (3DPBC) scaffolds using a translational, skeletally mature, large-animal calvarial defect model.

Materials and Methods—Custom 3DPBC scaffolds designed to present lattice-based porosity only towards the dural surface were either coated with collagen (control) or coated with collagen and immersed in a 100 μM concentration dipyridamole (DIPY) solution. Sheep (n=5) were subjected to 2 ipsilateral trephine-induced (11-mm diameter) calvarial defects. Either a control or a DIPY scaffold was placed in each defect, and the surgery was repeated on the contralateral side 3

Corresponding author: Paulo G. Coelho, 433 First Avenue, Room 844, New York, NY, 10010, United States of America, pc92@nyu.edu.

weeks later. Following sacrifice, defects were evaluated through microcomputed tomography and histologic analysis for bone, scaffold, and soft tissue quantification throughout the defect. Parametric and non-parametric methods were used to determine statistical significance based on data distribution.

Results—No exuberant or ectopic bone formation was observed, and no histologic evidence of inflammation was noted within the defects. Osteogenesis was higher in DIPY-coated scaffolds compared to controls at 3 weeks (p=0.013) and 6 weeks (p=0.046) *in vivo*. When bone formation was evaluated as a function of defect radius, average bone formation was higher for DIPY relative to control scaffolds at both time points (significant at defect central regions at 3 weeks and at margins at 6 weeks, p=0.046 and p=0.031, respectively).

Conclusion—Dipyridamole significantly improves the calvarial bone regeneration capacity of 3DPBC scaffolds. The most significant difference in bone regeneration was observed centrally within the interface between the 3DPBC scaffold and the dura mater.

Keywords

3D-printed; tissue engineering; calvaria; osteogenesis; dipyridamole

INTRODUCTION

Bone tissue engineering incorporates biomaterials that facilitate the genesis of osseous tissue. Work with bioactive ceramic-based approaches has included the use of compounds such as hydroxyapatite and β-tricalcium phosphate (β-TCP). However, the lack of a hierarchical approach when combining design parameters at the macro, meso, micro, and nano levels in their structure does not take full advantage of the opportunity to facilitate bone growth. To best leverage the osteoconductive properties of these biomaterials, custom-designed three-dimensionally printed bioactive ceramic (3DPBC) scaffolds can be created to fit and fill any size and shape defect with hierarchically organized configurations (Dutta Roy et al., 2003; Wilson et al., 2004).

An additional feature of any biomaterials-based construct designed for bone tissue engineering is the potential to further modulate the biomolecular pathways involved in bone formation. Adenosine receptor agonists have recently shown promising potential for enhancing osteogenesis, in particular via the adenosine A2A receptor (A2AR), which plays a pro-osteogenic role via osteoclast and inflammation inhibition and osteoblast activation (Costa et al., 2011; Mediero et al., 2012a; Mediero et al., 2013; Mediero et al., 2015). The augmentation of osteogenesis by the indirect A2AR agonist dipyridamole, a compound that increases local extracellular adenosine levels by inhibiting its uptake via Ent1, has been demonstrated in several studies (Costa et al., 2011; Mediero et al., 2012a; Mediero et al., 2013). The application of this agent within the craniomaxillofacial skeleton has been previously performed in a murine model, with dipyridamole-coated 3DPBC scaffolds used to fill cranial defects enhancing bone regeneration as effectively as BMP-2 (Ishack et al., 2017), without the above-described concerning effects of BMPs reported in the literature, such as osteolysis, ectopic bone formation, and craniosynostosis (Spiro et al., 2010; Carragee et al., 2011; Kinsella et al., 2011; Mediero et al., 2016).

The opportunity to leverage dipyridamole's osteogenic effects expands the potential applications of 3DPBC scaffolds. From a tissue regeneration standpoint, elucidating the effects of osteogenic signals on different tissue sources is highly desirable, as bone margin-, periosteal-, and dura-mediated healing alone is not sufficient, and incomplete defect regeneration is achieved (Petite et al., 2000; Li et al., 2016). To date, the only work combining 3D-printed constructs with dipyridamole in the calvarium has been performed in murine models (Ishack et al., 2017). While favorable results were obtained, no attempt was made to isolate the effect of dipyridamole on different bone healing tissue contributors (bone defect margin, dura, pericranium) due to the model's constraints in size. Therefore, in this study, using a sheep model, scaffolds designed to minimize/eliminate the infiltration of pericranium- and bone margin-derived osteogenic tissue while allowing for contact between the dura and an open, porous, lattice-based interior scaffold structure were used to test the effect of dipyridamole in bone generation in calvarial defects.

MATERIALS AND METHODS

Scaffold design and preparation

A 3DPBC scaffold composed of 100% β-TCP was designed and printed for inlay reconstruction of a surgically induced calvarial defect. Using RoboCAD 4.3 (3D Inks LLC, Tulsa, OK, USA), a circular scaffold was created with a 9-mm core and a cap that extended an additional 1 mm in all directions, for an overall scaffold diameter of 11 mm (Figure 1A–C). The scaffold core had an inner lattice network composed of cylindrical rods spaced ~330 μm apart, yielding a pore fraction of approximately 43%. In addition, the scaffolds possessed solid, 500-μm-thick outer walls, and solid, 500-μm-thick caps to prevent downward growth of the pericranium, leaving the dural side as the only face of the scaffold open and exposed to the local cellular and biochemical environment. The rationale for such scaffold design was to harness the non-porous nature of the scaffold wall and cap to limit the ability of soft tissue to infiltrate the surgical wound site during the early stages of healing.

Prior to implantation, scaffolds were coated with collagen by immersion in a 2% type I bovine collagen solution (Corning Inc., Corning, NY, USA). Half of the collagen-coated scaffolds were treated in a 100-μM dipyridamole (DIPY) solution (experimental group). This was created by a 1:100 dilution of 5.04 mg of dipyridamole in 1 mL of dimethyl sulfoxide (DMSO) with 1x phosphate-buffered saline (PBS), a choice guided by our preliminary work demonstrating the ability of this immersion concentration to enhance bone growth in an *in vivo* setting (Ishack et al., 2017), while the remaining scaffolds were left untreated aside from collagen coating (control group).

Surgical intervention and in vivo testing of 3DPBC scaffolds

The experimental cohort consisted of five skeletally mature Dorset/Finn sheep weighing approximately 62 kg at the time of the first operation. The osteogenic capability of the 3DPBC scaffolds was tested using two time points (3 and 6 weeks). Surgical intervention involved 2 separate operations performed 3 weeks apart, following a protocol approved by the Institutional Animal Care and Use Committee (IACUC). The left side of the calvarium was designated as the 6-week time point, while the right side served as the 3-week site.

The sheep were anesthetized with Telazol® and isoflurane. Following aseptic preparation of the surgical site over the calvarium, dissection was performed down to the periosteum. A trephine burr (10-mm inner diameter, 11-mm outer diameter) (Hu-Friedy Manufacturing Co., Chicago, IL, USA) was then used to make full-thickness anterior and posterior defects in the parietal bone spaced approximately 1 cm apart. Scaffolds placed in the anterior and posterior calvarial defects were designed to serve as control and DIPY groups, respectively. Scaffolds were inset with the cap at the most superior aspect of the defect (Figure 1D). The pericranium and scalp were then closed with running 4-0 nylon sutures. The sheep were given oxytetracycline 10 mg/kg as prophylaxis against infection and taken to recovery. Post-operatively, food and water *ad libitum* were offered to the animals. The surgery was repeated 3 weeks later on the contralateral side. An additional 3 weeks after this second surgery, the animals were humanely euthanized by anesthesia overdose, and the sheep calvaria were harvested by sharp dissection.

Sample preparation

Samples were initially placed in 70% ethanol and subjected to microcomputed tomography (microCT; μCT 40, SCANCO Medical, Bassersdorf, Switzerland). Each was then processed for histological evaluation via progressive dehydration in ethanol (70–100%) and methyl salicylate prior to final embedding and polymerization in methylmethacrylate (MMA). Non-decalcified histological sections were prepared for each defect according to standardized methodology (Campos et al., 2012; Jimbo et al., 2014).

A Buehler IsoMet saw (Buehler, Lake Bluff, IL, USA) was used to obtain ~100-μm-thick histological sections, which were polished to a 1200-grit finish. A 1-μm polishing compound was used to remove residual scratches and to obtain a final thickness of ~95 μm. A Stevenel blue and Van Gieson picro fuchsin differential tissue staining protocol (SVG) was used for staining the sections. SVG stains soft tissue green–blue and mineralized tissue red–orange, while the scaffold material stains orange–brown. The stained sections (one per sample from the central-most segment of the scaffold) were examined using a histology slide scanning system (Aperio Technologies, Vista, CA, USA).

Data analysis

Histomorphometry was performed using Adobe Photoshop CS5® (Adobe Systems Incorporated, San Jose, CA, USA) to delineate and to quantify the individual tissue types contained in each slide. We examined the histologic field within each sample in three different ways (regions of interest): (1) the distance, with the cap excluded, between the defect margin on each side and the outer boundary of the scaffold wall (Margins); (2) the peripheral 25% of the width of the scaffold's core on each side, with the cap and walls excluded (Outer Core); and (3) the interior 50% of the width of the scaffold's core (Inner Core) (Figure 2). Once this was complete, JVAnalysis 2014 (New York University Department of Biomaterials, New York, NY, USA) was used to quantify the percentages of bone, scaffold, and soft tissue.

Statistical considerations

All statistical analyses were performed with SPSS 23.0 (IBM Corp., Armonk, NY, USA). All data were assessed for normality using the Shapiro-Wilk test (p>0.05) prior to any analysis. Friedman tests were used for comparison of data sets that failed the normality test, and a linear mixed model was used for comparisons of data sets that met the Shapiro-Wilk normality test. Significance was set at an α =0.05.

RESULTS

Qualitative histologic observations

Histologic examination following SVG staining revealed no signs of ectopic bone growth or inflammation in either the DIPY or control samples at 3 or 6 weeks (Figures 3–6). At 3 weeks, deposition of osteoid and woven bone formation could be seen in both DIPY and control samples (Figures 3 and 4). Such woven bone formation was primarily observed within the space between the trephined margins and the scaffold's solid wall (Figures 3B and 4B). New bone formation was also observed in direct contact with the outer aspect of the wall, and initial bone formation was observed internally in direct proximity with the scaffold's solid wall for both DIPY and control groups (Figures 3B and 4B). At the central region of interest, only DIPY scaffolds showed initial formation of woven bone that initiated at the interface between the dura and the scaffold porous structure (Figure 4C).

At 6 weeks, samples demonstrated further bone healing, with initial replacement of woven bone by lamellar structures (Figures 5 and 6). Extensive bone deposition was observed between the osteotomized edges of the defect and the solid walls of the scaffold (Figures 5B and 6B). Within the interior of the scaffold, bone formation along the scaffold struts was qualitatively greater in the DIPY group relative to the control (Figures 5C and 6C).

Bone did not notably penetrate the walls or cap of the scaffold at both pericranial and defect margin flanges, both of which were composed of solid β-TCP. Despite this design feature included to minimize growth from the bony margins toward the center of the defect, a substantial percentage of surface area was occupied by osseous tissue organized around the struts of the lattice in the center of the scaffolds for both groups at this later time point.

Histomorphometric analysis

Prior to the quantification of the percentage of bone in each sample, sections of undisturbed sheep calvaria were evaluated to determine the baseline natural bone spatial occupancy, which was found to be 75.5%. With the understanding that bone only fills on approximately three-quarters of space within the unoperated sheep calvarium, results are presented as the percentage of bone occupancy under unoperated conditions. Thus, results are reported as a percentage between 0% and 100% of the baseline bone spatial occupancy.

When grouped based on *in vivo* time point, the percentage of bone at 6 weeks, averaged across the three regions of interest (Margins, Outer Core, Inner Core), was significantly greater than that seen at 3 weeks (22.2% vs. 4.8%; p<0.001). When averaged across region of interest and collapsed across time point, the Friedman statistical test indicated that bone

formation was significantly higher in defects with DIPY-coated scaffolds compared to controls (p=0.012). Estimated means and 95% confidence intervals for the overall percentage of bone present in our samples with bone and scaffold considered, collapsed across the three regions of interest and grouped by time point after implantation and coating with DIPY or collagen alone (control), are presented in Figure 7. The Friedman statistical test revealed that DIPY-coated scaffolds had significantly greater bone formation than controls at the 3-week time point (p=0.013). At 6 weeks *in vivo*, the mean percentage of bone surface area occupancy was ~70% higher in the DIPY group, a difference that achieved statistical significance (p=0.046).

Values for means and 95% confidence intervals of bone percentage for all samples, grouped by region of interest, time point, and DIPY or control are displayed in Figure 8. The average percentage of surface area occupied by bone was higher in the DIPY-coated samples for every region of interest at both time points. At 3 weeks, a significant effect of DIPY in early osteogenesis was detected at the center of the defect (Inner Core region) (p=0.046, Friedman statistical test). At 6 weeks, within the region of interest closest to the defect edges (Margins), DIPY-coated samples had significantly higher (p=0.031), ~70% more occupancy by osseous tissue than controls (Figure 8A). Likewise, bone surface area occupancy was ~55% and >85% greater in the DIPY group at this latter time point within the region defined by the inner bounds of the scaffold wall and the outer 25% of the scaffold core's diameter on each side (Outer Core) and the inner 50% of the scaffold diameter (inner core), respectively (Figures 8B and 8C).

DISCUSSION

The reconstruction of calvarial defects is a common challenge associated with the treatment of congenital anomalies, craniofacial trauma, and oncologic surgery. Autogenous bone, a common first-line treatment, is limited by a finite supply and donor site morbidity (Kuik et al., 2016; Costa Mendes et al., 2016), creating a need for alternative therapies that circumvent the drawbacks to bone grafting. Bone tissue engineering presents a potential solution through utilizing biomaterials-based osteoconductive strategies, often in conjunction with manipulation of the biomolecular processes of bone formation. However, the ideal approach to regenerating vascularized, autogenous bone through tissue engineering is yet to be developed (Kinoshita and Maeda, 2013).

In this study, we present an experiment designed to challenge the ability of a tissue engineering scaffold coated by a pharmacologic agent to enhance the reconstruction of calvarial bone defects. While the resolution of current three-dimensional printers has improved substantially, the incorporation of large lattice-based porosity structures known to increase bone regeneration that also incorporate solid barriers to minimize pericranium- and bone defect margin-derived healing within miniature calvarial scaffolds in murine models is currently unfeasible. Dimensional constraints in murine models result not only in reduced dura-scaffold interfacial area for analysis, but also in reduced distances between the solid walls and central regions of the defect. Such limitations were circumvented through the use of a large translational animal model. Traditional techniques of calvarial reconstruction rely on autologous bone grafting or the use of synthetic implantable devices. While these

treatment options have been the cornerstones of care for decades, they have known limitations. Autologous bone is a finite resource, may be insufficient to reconstruct larger defects, can resorb over time, and is associated with donor site morbidity. (Kuik et al., 2016; Costa Mendes et al., 2016) Implantable devices including titanium meshes and synthetic prostheses made from materials such as methylmethacrylate (MMA), polyetheretherketone (PEEK), and porous polyethylene can cover a sizeable area and be customized to each patient. However, there are drawbacks that may include device exposure, extrusion, infection, and need for replacement in the growing skull (Sahoo et al., 2010; Ng et al., 2014). Therefore, keeping with Millard's concept of replacing tissue losses in kind (Millard Jr, 1986), the field of bone tissue engineering aims to stimulate the formation of native bone.

Biomaterials such as β-TCP provide an osteoconductive foundation in bone tissue engineering. Although much has already been done to understand the inherent properties of β-TCP (Biskup et al., 2010), improvement upon the design of scaffolds used in the calvarium is possible. The application of 3D-printed scaffolds, as described in this work, provides a rigid, space-occupying construct. The biomaterials-based scaffold presents osteoconductive surfaces in close contact with cut bony edges of the calvarium and dura mater. The importance of maintaining separation between the dura and pericranium to limit soft tissue invasion of the defect site that could impair healing has previously been described (Gosain et al., 2003) and is further supported by our results. By using a design with a solid cap and walls, we attempted to isolate different areas of our calvarial defect to independently assess patterns of bone healing in these regions, such as minimizing the interference of pericranium- and bone defect margin-derived healing at the interface between the dura and the lattice-based inferior surface of the scaffold.

The primary objective of this experiment was to test the ability of the indirect A2AR agonist dipyridamole to enhance osteogenesis in cranial defects when added to 3DPBC scaffolds. Through blockage of the Ent1 transporter, dipyridamole increases local extracellular adenosine levels and promotes activation of the A2AR (Costa et al., 2011), which in turn promotes the formation of bone through a number of mechanisms such as the blockage of osteoclast differentiation (Mediero et al., 2012a; Mediero et al., 2013) and function (Mediero et al., 2012b), while simultaneously increasing osteoblast proliferation as well as the expression of osteogenic markers including osteocalcin and osteonectin (Mediero et al., 2013).

However, the use of dipyridamole for the purposes of harnessing its osteogenic potential represents a departure from its historical applications. Known commercially as Persantine®, dipyridamole has a decades-long history of safe use in adult as well as pediatric patients as an antithrombotic and vasodilatory medication, and often serves as the agent of choice for pharmacologic cardiac stress testing. When prescribed for daily use, it is administered systemically in doses of 75–100 mg every 6 hours in adults, and 2–5 mg/kg every 8 hours in children (FitzGerald, 1987; Patrono et al., 1998; Monagle et al., 2012). In contrast, ~100 mL of the 100 μM solution in which our scaffolds are immersed contains only ~5 mg of dipyridamole, of which only a fraction is absorbed by the construct prior to its placement into each bony defect.

Adverse events associated with dipyridamole are generally mild, and overall the drug is associated with a favorable side effect profile. As with any antithrombotic agent, the threat of excessive bleeding exists. However, in a large study of patients taking dipyridamole at a dose of 200 mg orally twice per day for secondary stroke prevention, less than 5% of patients experienced an episode of uncontrolled or pathologic bleeding, while this risk was nearly doubled in those taking aspirin (Diener et al., 1996). Other side effects linked to dipyridamole include those related to its vasodilatory properties, such as headache and dizziness as well as gastrointestinal disturbances including dyspepsia, nausea, or diarrhea (Diener et al., 1996). Furthermore, aside from a single report of an increased risk of non-osteoporotic fractures, no evidence exists of any adverse effects on immature or mature skeletal structures in patients taking oral or intravenous dipyridamole (Vestergaard et al., 2012). With this knowledge, in conjunction with results from prior studies (Costa et al., 2011; Mediero et al., 2012a; Mediero et al., 2013; Mediero et al., 2015; Ishack et al., 2017), the safe and efficacious application of dipyridamole in the field of bone tissue engineering is a conceivable goal.

In the present study, dipyridamole contributed to an overall significant increase in bone formation within our cranial defect when both times *in vivo* and all three regions of interest were included in the analysis. When comparisons were performed including all regions of interest as a function of time *in vivo*, differences were significant at 3 weeks *in vivo* and marginally significant at 6 weeks *in vivo* in favor of DIPY-containing samples. Further analysis of the data showed that DIPY increased bone formation at every region of interest at both times in vivo, with the highest increase (greater than 85% relative to control) in osteogenesis in the central-most region of the calvarial defect. The scaffold design allowed for findings that are strongly indicative of a positive effect of dipyridamole in hastening healing at regions where both the dura and instrumented bone margins were available for healing (Margins) and in regions where only the dura surface was the main osteogenic tissue source (Outer Core and Inner Core). Such findings are of special interest in cases of extensive defects or when one or more osteogenic sources may be compromised, such as following oncologic resection or traumatic injury (Gosain et al., 2003).

Prior work in rat models found that the dura's osteogenic capacity is based at the molecular level in proliferation and production of growth factors and extracellular matrix molecules such as transforming growth factor β-1 (TGF-β1) and osteocalcin. Additionally, the presence of alkaline phosphatase-positive cells cultured from immature rat dura mater suggests its capacity to contribute osteoblastic content to the process of calvarial bone regeneration (Greenwald et al., 2000a; Greenwald et al., 2000b). While the exact nature and extent of the interplay between dipyridamole and the dura has not yet been addressed in detail, previous studies have unequivocally demonstrated higher osteoblastic and lower osteoclastic gene expression in murine calvarial bones and found that dipyridamole acts via the A2AR to promote precursor cell differentiation and to enhance pro-osteogenic influences.

The 11-mm calvarial defects created have been shown to be subcritical, smaller than a previously described critical size of 22 mm (Viljanen et al., 1997). However, our study was designed to examine patterns of bone healing of 3DPBC scaffolds in response to

dipyridamole. Furthermore, we minimized pericranium- and bone-mediated healing in an attempt to isolate dural-mediated calvarial healing within the defect center. While the results of the present study strongly indicate the ability of dipyridamole to hasten initial bone healing in a large translational preclinical model, substantial work is warranted for the adequate development of an informed design platform for calvarial bone healing. To refine the contributions of different tissues to calvarial bone healing, an increase in sample size and the inclusion of several groups are warranted. These include empty defects (no scaffold), empty and scaffold-filled defects with isolation of the scaffold from the dura, as well as permutations of scaffold wall closure/openness with and without isolation from the dura. Furthermore, inclusion of longer post-operative healing periods would be informative with respect to the progression of bone growth and scaffold degradation, and will also be a subject of future studies.

CONCLUSION

In this study, dipyridamole improved the calvarial bone regeneration capacity of 3D-printed bioactive ceramic scaffolds, as a significant increase in bone formation across all regions was observed in dipyridamole-containing samples relative to controls at both 3 and 6 weeks postoperatively. The most significant difference in bone regeneration was observed centrally within the interface between the 3DPBC scaffold and the dura mater, where a greater than 85% increase in bone formation was observed compared to control scaffolds at the 6-week time point. Additionally, the absence of ectopic or overly exuberant bone formation as well as evidence of an inflammatory reaction suggest the safety of dipyridamole as applied within this study.

Acknowledgments

References

Biskup NI, Singh DJ, Beals S, Joganic EF, Manwaring K. Pediatric cranial vault defects: early experience with beta-tricalcium phosphate bone graft substitute. J Craniofac Surg. 2010; 21:358–62. [PubMed: 20186087]

Campos FE, Gomes JB, Marin C, et al. Effect of drilling dimension on implant placement torque and early osseointegration stages: an experimental study in dogs. J Oral Maxillofac Surg. 2012; 70:e43–50. [PubMed: 22182660]

Carragee EJ, Hurwitz EL, Weiner BK. A critical review of recombinant human bone morphogenetic protein-2 trials in spinal surgery: emerging safety concerns and lessons learned. Spine J. 2011; 11:471–91. [PubMed: 21729796]

Costa MA, Barbosa A, Neto E, et al. On the role of subtype selective adenosine receptor agonists during proliferation and osteogenic differentiation of human primary bone marrow stromal cells. J Cell Physiol. 2011; 226:1353–66. [PubMed: 20945394]

Costa Mendes L, Sauvigne T, Guiol J. [Morbidity of autologous bone harvesting in implantology: Literature review from 1990 to 2015]. Morbidite des prelevements osseux autogenes en implantologie: revue de litterature de 1990a 2015. Rev Stomatol Chir Maxillofac Chir Orale. 2016; 117:388–402. [PubMed: 27825665]

Diener HC, Cunha L, Forbes C, Sivenius J, Smets P, Lowenthal A. European Stroke Prevention Study. 2. Dipyridamole and acetylsalicylic acid in the secondary prevention of stroke. J Neurol Sci. 1996; 143:1–13. [PubMed: 8981292]

Dutta Roy T, Simon JL, Ricci JL, Rekow ED, Thompson VP, Parsons JR. Performance of hydroxyapatite bone repair scaffolds created via three-dimensional fabrication techniques. J Biomed Mater Res A. 2003; 67:1228–37. [PubMed: 14624509]

FitzGerald GA. Dipyridamole. N Engl J Med. 1987; 316:1247–57. [PubMed: 3553945]

Gosain AK, Santoro TD, Song LS, Capel CC, Sudhakar PV, Matloub HS. Osteogenesis in calvarial defects: contribution of the dura, the pericranium, and the surrounding bone in adult versus infant animals. Plast Reconstr Surg. 2003; 112:515–27. [PubMed: 12900610]

Greenwald JA, Mehrara BJ, Spector JA, et al. Biomolecular mechanisms of calvarial bone induction: immature versus mature dura mater. Plast Reconstr Surg. 2000a; 105:1382–92. [PubMed: 10744229]

Greenwald JA, Mehrara BJ, Spector JA, et al. Immature versus mature dura mater: II. Differential expression of genes important to calvarial reossification. Plast Reconstr Surg. 2000b; 106:630–8. discussion 9. [PubMed: 10987470]

Ishack S, Mediero A, Wilder T, Ricci JL, Cronstein BN. Bone regeneration in critical bone defects using three-dimensionally printed beta-tricalcium phosphate/hydroxyapatite scaffolds is enhanced by coating scaffolds with either dipyridamole or BMP-2. J Biomed Mater Res B Appl Biomater. 2017; 105:366–75. [PubMed: 26513656]

Jimbo R, Tovar N, Marin C, et al. The impact of a modified cutting flute implant design on osseointegration. Int J Oral Maxillofac Surg. 2014; 43:883–8. [PubMed: 24583140]

Kinoshita Y, Maeda H. Recent developments of functional scaffolds for craniomaxillofacial bone tissue engineering applications. Sci World J. 2013; 2013:863157.

Kinsella CR Jr, Cray JJ, Durham EL, et al. Recombinant human bone morphogenetic protein-2-induced craniosynostosis and growth restriction in the immature skeleton. Plast Reconstr Surg. 2011; 127:1173–81. [PubMed: 21364420]

Kuik K, Putters TF, Schortinghuis J, van Minnen B, Vissink A, Raghoebar GM. Donor site morbidity of anterior iliac crest and calvarium bone grafts: a comparative case-control study. J Craniomaxillofac Surg. 2016; 44:364–8. [PubMed: 26857759]

Li CS, Yang P, Ting K, et al. Fibromodulin reprogrammed cells: a novel cell source for bone regeneration. Biomaterials. 2016; 83:194–206. [PubMed: 26774565]

Mediero A, Kara FM, Wilder T, Cronstein BN. Adenosine A(2A) receptor ligation inhibits osteoclast formation. Am J Pathol. 2012a; 180:775–86. [PubMed: 22138579]

Mediero A, Frenkel SR, Wilder T, He W, Mazumder A, Cronstein BN. Adenosine A2A receptor activation prevents wear particle-induced osteolysis. Sci Transl Med. 2012b; 4:135ra65.

Mediero A, Perez-Aso M, Cronstein BN. Activation of adenosine A(2A) receptor reduces osteoclast formation via PKA- and ERK1/2-mediated suppression of NFkappaB nuclear translocation. Br J Pharmacol. 2013; 169:1372–88. [PubMed: 23647065]

Mediero A, Wilder T, Perez-Aso M, Cronstein BN. Direct or indirect stimulation of adenosine A2A receptors enhances bone regeneration as well as bone morphogenetic protein-2. FASEB J. 2015; 29:1577–90. [PubMed: 25573752]

Mediero A, Wilder T, Reddy VS, et al. Ticagrelor regulates osteoblast and osteoclast function and promotes bone formation in vivo via an adenosine-dependent mechanism. FASEB J. 2016; 30:3887–900. [PubMed: 27511945]

Millard, D, Jr. Principalization of Plastic Surgery. Little Brown, Boston: 1986. p. 229-35.

Monagle P, Chan AK, Goldenberg NA, et al. Antithrombotic therapy in neonates and children: Antithrombotic Therapy and Prevention of Thrombosis, 9th ed: American College of Chest Physicians Evidence-Based Clinical Practice Guidelines. Chest. 2012; 141:e737S–801S. [PubMed: 22315277]

Ng ZY, Ang WJ, Nawaz I. Computer-designed polyetheretherketone implants versus titanium mesh (+/− acrylic cement) in alloplastic cranioplasty: a retrospective single-surgeon, single-center study. J Craniofac Surg. 2014; 25:e185–9. [PubMed: 24621767]

Patrono C, Coller B, Dalen JE, et al. Platelet-active drugs: the relationships among dose, effectiveness, and side effects. Chest. 1998; 114:470S–88S. [PubMed: 9822058]

Petite H, Viateau V, Bensaid W, et al. Tissue-engineered bone regeneration. Nat Biotechnol. 2000; 18:959–63. [PubMed: 10973216]

Sahoo N, Roy ID, Desai AP, Gupta V. Comparative evaluation of autogenous calvarial bone graft and alloplastic materials for secondary reconstruction of cranial defects. J Craniofac Surg. 2010; 21:79–82. [PubMed: 20061970]

Spiro AS, Timo Beil F, Baranowsky A, et al. BMP-7–induced ectopic bone formation and fracture healing is impaired by systemic NSAID application in C57BL/6-mice. J Orthop Res. 2010; 28:785–91. [PubMed: 20063306]

Vestergaard P, Steinberg TH, Schwarz P, Jorgensen NR. Use of the oral platelet inhibitors dipyridamole and acetylsalicylic acid is associated with increased risk of fracture. Int J Cardiol. 2012; 160:36–40. [PubMed: 21463909]

Viljanen VV, Lindholm TC, Gao TJ, Lindholm TS. Low dosage of native allogeneic bone morphogenetic protein in repair of sheep calvarial defects. Int J Oral Maxillofac Surg. 1997; 26:389–93. [PubMed: 9327294]

Wilson CE, de Bruijn JD, van Blitterswijk CA, Verbout AJ, Dhert WJ. Design and fabrication of standardized hydroxyapatite scaffolds with a defined macro-architecture by rapid prototyping for bone-tissue-engineering research. J Biomed Mater Res A. 2004; 68:123–32. [PubMed: 14661257]
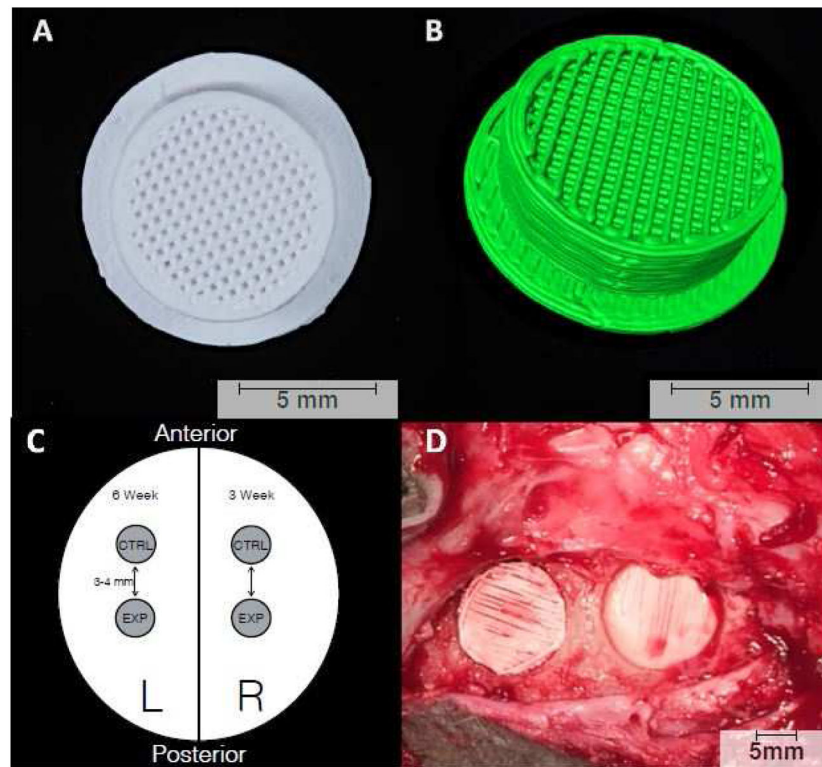
Figure 1.
3D-printed bioactive ceramic scaffold composed of β-tricalcium phosphate. (A) Inferior surface of the scaffold showcasing the porous core with central lattice. The scaffolds were placed in the trephine-induced calvarial defects such that this lattice-work faced the dura. (B) 3D reconstruction of the scaffold created using Amira 6.1 software (Visage Imaging GmbH, Berlin, Germany). (C) Schematic representation of experimental design showing location of placement for each study group and time point. (D) Intra-operative photograph showing scaffold placement in anterior and posterior calvarial defects.
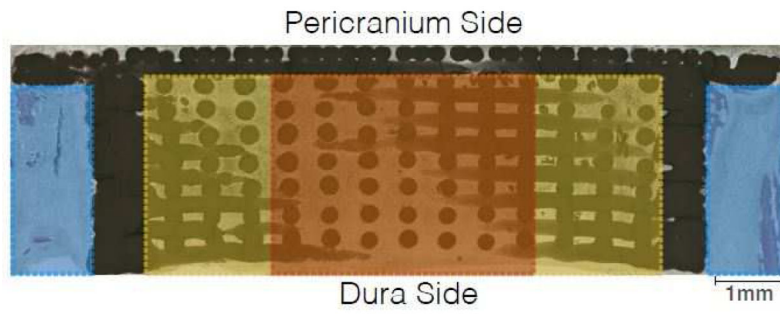
Figure 2.
Histologic image depicting the three different methods (Margins, Outer Core, Inner Core) used for analysis of tissue composition of experimental samples.
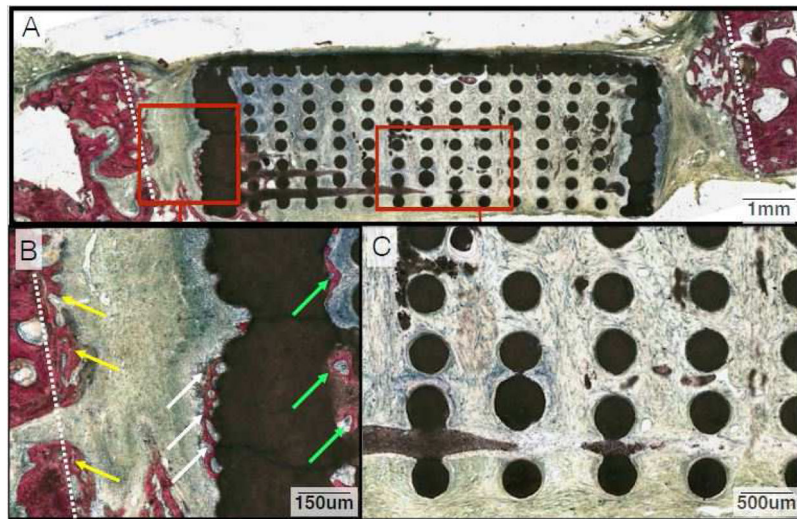
Figure 3.
(A) Representative histologic image from animals in the control group at the 3-week time point. (B) Close-up depicting osteoid deposition and woven bone growth between the defect margin and wall of the scaffold (Yellow Arrows). There is also a minimal amount of new bone forming along the outside (White Arrows) and inside of the scaffold wall (Green Arrows). (C) Magnification of the inner lattice of the scaffold. Note the paucity of osseous tissue inside the wall, particularly in comparison to that between the defect margin and the outside of the scaffold wall.
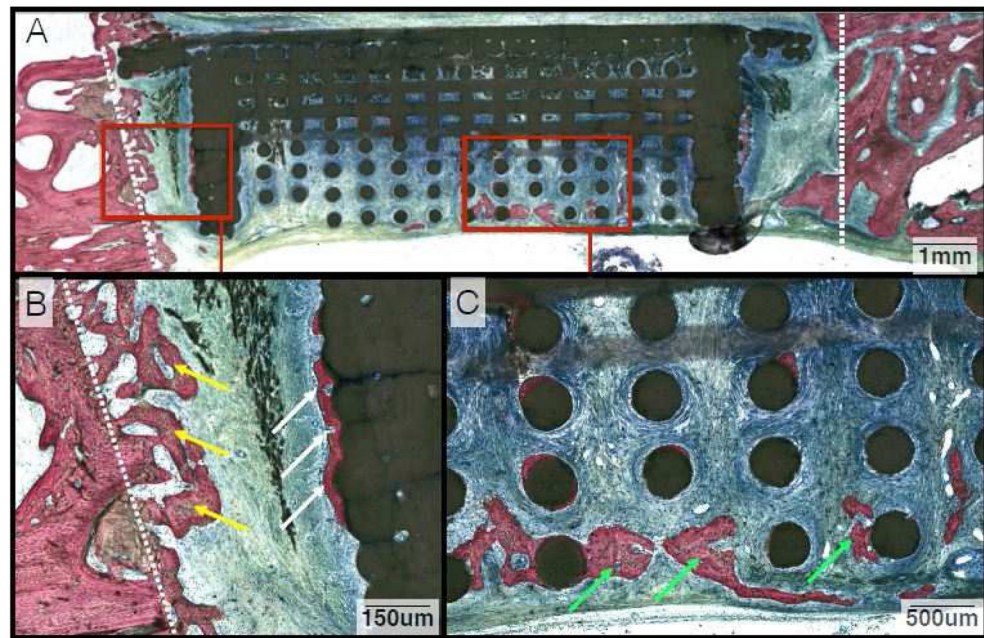
Figure 4.
(A) Representative histologic image from animals in the DIPY group at the 3-week time point. (B) Magnification of bone growth between the osteotomized edge of the defect (Yellow Arrows) and outer wall of the scaffold (White Arrows). (C) Close-up image of bone formation along the inner lattice of the scaffold (Green Arrows). While there is an increase in bone regeneration in the center of the defect relative to controls, it is limited in both groups at this earlier time point.
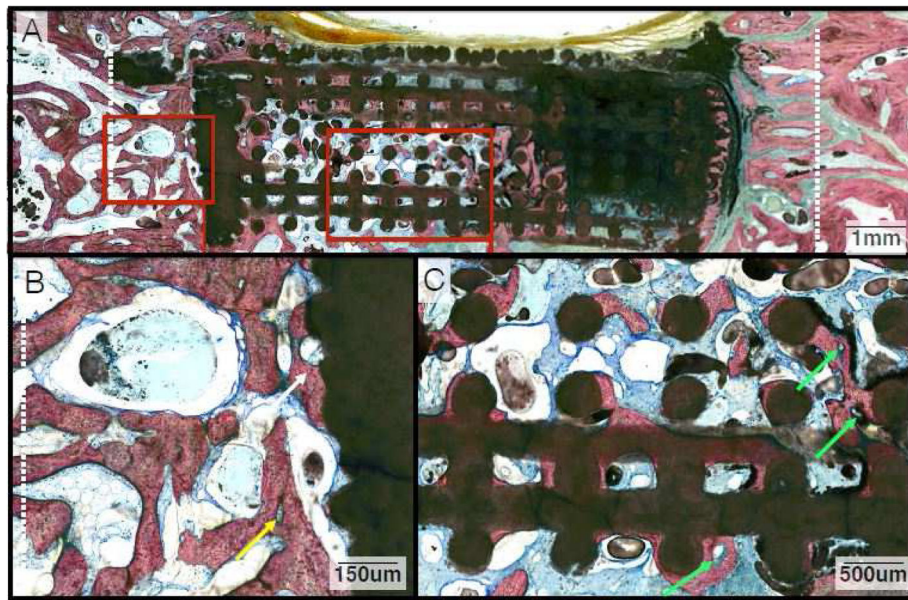
Figure 5.
(A) Representative histologic image from animals in the control group at the 6-week time point. (B) Magnification of abundant bone growth between the defect margin and wall of the scaffold (White Arrow) with a primary osteon highlighted (Yellow Arrow). (C) Along the inner lattice of the scaffold, woven bone is abundant and there is evidence of early remodeling with formation of osteons and angiogenesis (Green Arrows).
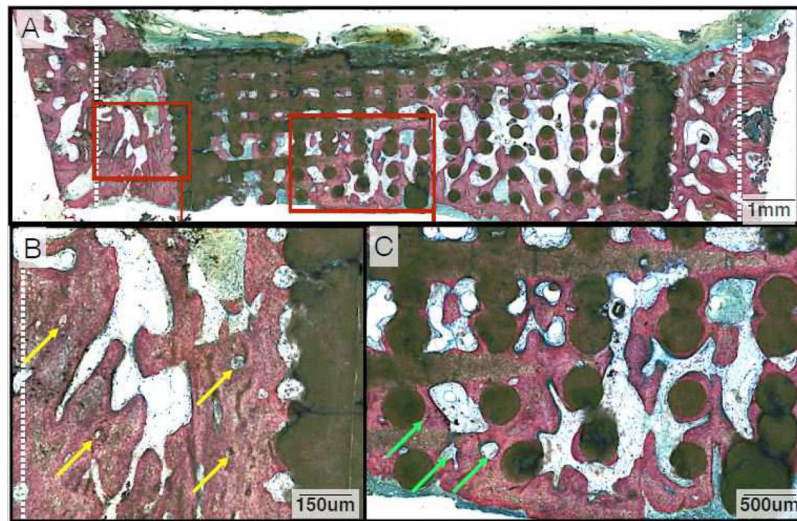
Figure 6.
(A) Representative histologic image from animals in the DIPY group at the 6-week time point. (B) Close-up depicting significant bony infill within the space between the defect margin and wall of the scaffold, with several osteons highlighted (Yellow Arrows) that provide evidence of lamellar reorganization. (C) Magnification of the extensive bone formation observed along the scaffold's inner lattice. Angiogenesis and osteon development is evident (Green Arrows) and more prevalent in the DIPY group compared to controls at this later time point.
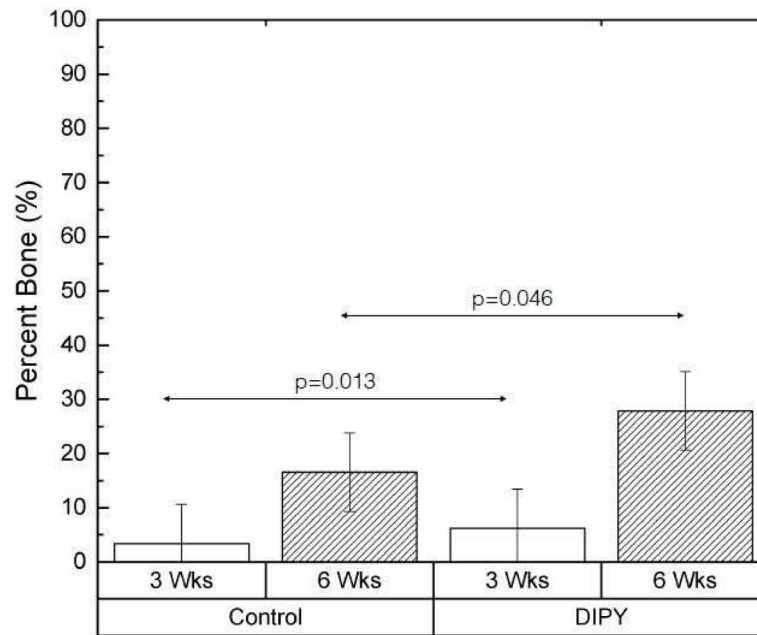
Figure 7.
Graph depicting the percentage of bone formation in each of our groups, averaged across all three methods of analysis (Margins, Outer Core, Inner Core). Samples are grouped by both DIPY or control status and time point. Bars represent means for each group and error bars indicate 95% confidence intervals.
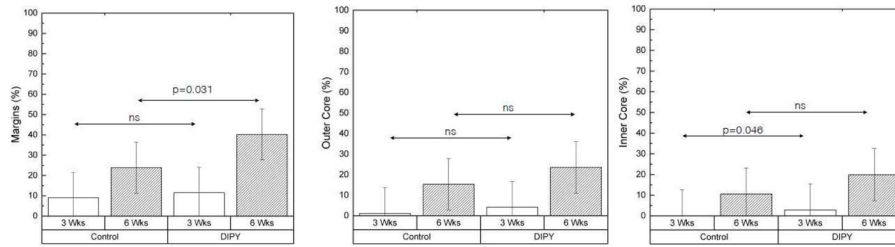
Figure 8.
Graphs showing the percentage of bone formation in each of our groups, broken down by individual regions of interest (A: Distance between defect margins and outer boundary of the scaffold wall [Margins], B: Peripheral 25% of the diameter of the scaffold core on each side with the cap and walls excluded [Outer Core], C: Middle 50% of the diameter of the scaffold core [Inner Core]) and grouped by DIPY or control as well as time point. Bars represent means for each group and error bars depict 95% confidence intervals.